The Phase Behavior of Cationic Lipid–DNA Complexes

Sylvio May, Daniel Harries, and Avinoam Ben-Shaul
Department of Physical Chemistry and the Fritz Haber Research Center, The Hebrew University of Jerusalem, Jerusalem 91904, Israel

ABSTRACT We present a theoretical analysis of the phase behavior of solutions containing DNA, cationic lipids, and nonionic (helper) lipids. Our model allows for five possible structures, treated as incompressible macroscopic phases: two lipid–DNA composite (lipoplex) phases, namely, the lamellar (L_α^C) and hexagonal (H_{II}^C) complexes; two binary (cationic/neutral) lipid phases, that is, the bilayer (L_α) and inverse-hexagonal (H_{II}) structures, and uncomplexed DNA. The free energy of the four lipid-containing phases is expressed as a sum of composition-dependent electrostatic, elastic, and mixing terms. The electrostatic free energies of all phases are calculated based on Poisson–Boltzmann theory. The phase diagram of the system is evaluated by minimizing the total free energy of the three-component mixture with respect to all the compositional degrees of freedom. We show that the phase behavior, in particular the preferred lipid–DNA complex geometry, is governed by a subtle interplay between the electrostatic, elastic, and mixing terms, which depend, in turn, on the lipid composition and lipid/DNA ratio. Detailed calculations are presented for three prototypical systems, exhibiting markedly different phase behaviors. The simplest mixture corresponds to a rigid planar membrane as the lipid source, in which case, only lamellar complexes appear in solution. When the membranes are "soft" (i.e., low bending modulus) the system exhibits the formation of both lamellar and hexagonal complexes, sometimes coexisting with each other, and with pure lipid or DNA phases. The last system corresponds to a lipid mixture involving helper lipids with strong propensity toward the inverse-hexagonal phase. Here, again, the phase diagram is rather complex, revealing a multitude of phase transitions and coexistences. Lamellar and hexagonal complexes appear, sometimes together, in different regions of the phase diagram.

INTRODUCTION

Mixing aqueous solutions containing DNA and cationic liposomes results in the spontaneous formation of composite, typically micron size, complexes containing both DNA and lipid molecules (Rädler et al., 1997; Koltover et al., 1998; Lasic et al., 1997; Templeton et al., 1997; Sternberg et al., 1994; Tarahovsky et al., 1996; Hübner et al., 1999; Boukhnikachvili et al., 1997; Pitard et al., 1999). These complexes are of great current interest as gene-delivery vectors, in which context they are sometimes called "lipoplexes" (Felgner et al., 1987; Felgner, 1997; Lasic, 1997; Hope et al., 1998). In general, the liposomes used for complex formation contain at least two kinds of lipid molecules. The key component are the cationic lipids (CL), which serve as the condensing agents of the negatively charged DNA strands. Also important are the neutral helper lipids (HL), which play a crucial role in determining the structure of the composite condensates. They also seem to affect the DNA transfection efficiency, yet their operation mechanism is not entirely clear (Hui et al., 1996; Zuidam et al., 1999).

The preferred equilibrium geometry of a lipid–DNA condensate is dictated by the surface charge density and the elastic properties of its constituent lipid layers. Both of these characteristics depend, in turn, on the nature and composition of the CL/HL mixture. Double-stranded DNA, being a rather rigid molecule (of large persistence length, $l_P \approx 500$ Å for B-DNA), imposes constraints on the possible lipoplex geometries because it retains its essentially linear structure in all complexes. In contrast, the lipid layers are soft self-assembled membranes that can adapt their structure to optimize the complexation geometry.

Indeed, several different lipoplex morphologies have been observed, corresponding to different lipid mixtures. Some of these structures may correspond to metastable intermediates, e.g., the spaghetti-like aggregates that consist of a (possibly supercoiled) double-stranded DNA wrapped around by the CL/HL bilayer (Sternberg et al., 1994; Sternberg, 1996; May and Ben-Shaul, 1997). Two condensate symmetries have been unambiguously identified as equilibrium ordered phases. These are the lamellar, L_α^C, and the hexagonal, H_{II}^C, aggregates, whose structural and thermodynamic characteristics have been quantitatively determined by x-ray diffraction and complementary measurements (Rädler et al., 1997; Salditt et al., 1997; Koltover et al., 1998; see also Lasic et al., 1997; Templeton et al., 1997; Tarahovsky et al., 1996; Hübner et al., 1999; Boukhnikachvili et al., 1997; Pitard et al., 1999).

The L_α^C (or "sandwich") phase is a smectic-like array of stacked lipid bilayers with DNA monolayers intercalated within the intervening water gaps. The DNA strands within each gallery are parallel to each other, exhibiting a definite repeat distance d. Although d depends on the CL/DNA and CL/HL concentration ratios, the spacing between two apposed lipid monolayers is nearly constant, $l \approx 26$ Å, corresponding to the diameter of a double stranded B-DNA ($2R_D \approx 20$ Å) surrounded by a thin hydration layer. The L_α^C

Received for publication 13 August 1999 and in final form 5 January 2000.
Address reprint requests to Avinoam Ben-Shaul, Dept. of Physical Chemistry and the Fritz Haber Research Center for Molecular Dynamics, The Hebrew Univ. of Jerusalem, Jerusalem 91904, Israel. Tel.: +972-2-658-5271; Fax: +972-2-651-3742; E-mail: abs@fh.huji.ac.il.

0006-3495/00/04/1681/17 $2.00

phase is stabilized by the electrostatic attraction between the negatively charged DNA and the cationic lipid bilayer. Without DNA, the lamellar lipid phase (L_α) is unstable owing to the strong electrostatic repulsion between the charged bilayers.

Similarly, the H_{II}^C, or "honeycomb" (May and Ben-Shaul, 1997), structure may be regarded as an ordinary inverse-hexagonal (H_{II}) lipid phase with DNA strands intercalated within its water tubes. Here too, the diameter of the water tubes is just slightly larger than the diameter of the DNA rods. The presence of DNA is crucial for stabilizing the hexagonal structure. Without it, strong electrostatic repulsions will generally drive the lipids to organize in planar bilayers.

The structural differences between the L_α^C and H_{II}^C phases imply significant differences between the electrostatic (charging) energies and the lipid elastic energies of these two geometries. In the H_{II}^C phase, each DNA molecule is surrounded by a highly (negatively) curved lipid monolayer, of radius $R \approx 13$ Å (Koltover et al., 1998). This cylindrically concentric geometry provides efficient neutralization of the DNA charges by the cationic surface charges, especially at the isoelectric point, where the total cationic charge exactly balances the total DNA charge (May and Ben-Shaul, 1997). In contrast, the strongly bent lipid monolayer may inflict a significant curvature deformation energy penalty. The lower the bending rigidity of the monolayer, k, the smaller the deformation free energy price (Helfrich, 1973). More favorable is the case where c_0, the spontaneous curvature of the monolayer, conforms to the curvature of the DNA rod, namely, $-c_0 \simeq 1/R_D$, (the minus sign signifying that the monolayer curvature is opposite that of the DNA). Under these circumstances, the hexagonal complexes are expected to be more stable than the lamellar ones. It must be noted, however, that charged lipids generally prefer the planar bilayer geometry ($c_0 \approx 0$), whereas the inverse-hexagonal geometry is preferred by (some) neutral lipids. Thus, the stability of H_{II}^C complexes is expected to depend sensitively on lipid composition. Similar qualitative considerations imply that lipid mixtures characterized by a high bending stiffness ($k \gg k_BT$ where k_B is Boltzmann's constant and T the temperature) and/or small spontaneous curvature ($|c_0| \ll 1/R_D$) will favor the formation of the L_α^C phase (May and Ben-Shaul, 1997; Harries et al., 1998; Koltover et al., 1998). In this geometry, charge matching is somewhat less efficient than in the hexagonal packing, yet the lower curvature energy overrides this difference.

These qualitative notions were elegantly corroborated by recent experiments in which the elastic properties of the lipid monolayers were controlled by changing the nature of the lipid mixture (Koltover et al., 1998). The cationic lipid in these experiments, dioleoyl trimethylamonium propane (DOTAP), is characterized by a very small spontaneous curvature. Using mixed-lipid vesicles composed of DOTAP as the cationic lipid and dioleoyl phosphatidylethanolamine (DOPE) as the helper lipid, it was found that the preferred aggregation geometry is the H_{II}^C phase. In contrast, using dioleoylphosphatidylcholine (DOPC) as the helper lipid promotes the formation of L_α^C complexes. These findings are consistent with the fact that pure DOPE self-organizes into an H_{II} phase, i.e., the spontaneous curvature of this lipid is negative, whereas DOPC molecules prefer the formation of planar bilayers. In these experiments, one tunes the spontaneous curvature of the lipid layer by controlling the composition of the lipid mixture. Based on many experiments in microemulsion systems, it is known that one can also control the bending rigidity of amphiphilic films. For example, by adding short chain alcohols to the mixture, it is possible to reduce the bending rigidity by about one order of magnitude (Safinya et al., 1989; Szleifer et al., 1988). Indeed, the addition of hexanol to the DOTAP/DOPC-DNA system results in a clear, first-order, $L_\alpha^C \rightarrow H_{II}^C$ phase transition (Koltover et al., 1998).

The qualitative considerations outlined above regarding the relative stabilities of different CL-DNA aggregates apply to one, given, CL/HL composition. Furthermore, they are only valid if all lipids and DNA molecules participate in complex formation. Different considerations apply when the mixture is nonstoichiometric. Taking into account that aqueous solutions containing DNA and two kinds of lipids are multicomponent systems, they are expected to exhibit rich and complex phase behaviors.

For a given salt concentration (chemical potential) the aqueous solution can be treated as a large reservoir embedding the condensed phases (i.e., complexes, bare bilayers, and naked DNA), allowing one to count out the water and salt. This leaves us with three relevant chemical species (CL, HL, and DNA) which, by Gibbs' phase rule, corresponds to (a maximum of) five thermodynamic degrees of freedom. Fixing the temperature and assuming that the lipid layers are incompressible (in all four lipid-containing phases), we eliminate two more degrees of freedom. Still, the phase rule implies that (up to) three condensed phases can coexist in solution, e.g., two kinds of complexes and uncomplexed DNA. The experimental observation of a first-order $L_\alpha^C \rightarrow H_{II}^C$ transition (Koltover et al., 1998), i.e., two coexisting phases, is in line with this conclusion. As we shall see, these systems are also expected to exhibit three-phase equilibria.

Our goal in this paper is to analyze theoretically the major determinants of the phase behavior of lipid–DNA solutions. To this end, we have studied in detail several representative systems, corresponding to lipid mixtures of different elastic characteristics. As we shall see, the phase behavior is quite simple for lipid layers which, in the absence of DNA, show strong propensity to form planar bilayers. Much richer and more complex phase diagrams, involving a multitude of transitions and coexistence regimes, are predicted for flexible and/or curvature loving lipid layers.

The phase diagrams presented in the following sections involve two levels of calculations. First, for a given type of lipid mixture, we calculate, as a function of the lipid composition (CL ratio) and lipid/DNA ratio, the elastic, mixing, and electrostatic charging free energies of all relevant structures, i.e., the L_α^C and H_{II}^C complexes, the bilayer and inverse-hexagonal lipid phases, and the uncomplexed DNA, as illustrated in Fig. 1. (The symbols H for H_{II}^C etc. are used for notational brevity.)

The electrostatic free energies are calculated based on the nonlinear Poisson–Boltzmann (PB) equation using methods described elsewhere (May and Ben-Shaul, 1997; Harries et al., 1998). The elastic terms are evaluated using familiar expressions for the curvature and stretching deformations and simple models for the elastic constants of mixed lipid monolayers. Then, writing the total free energy of the solution as a weighted sum involving all possible phases, we determine the phase diagram by minimizing this free energy with respect to all relevant thermodynamic variables.

THEORY

We consider an aqueous salt solution containing N^+ (monovalent) cationic lipids, N^0 helper lipids, and double-stranded DNA of total charge $-eM$, e denoting the elementary charge. The lipid and DNA molecules are distributed among the five possible structures shown in Fig. 1. We assume that all these structures, including the naked DNA, are large enough and can thus be treated as macroscopic phases. The total volume fraction of the condensed phases is assumed to be small, enabling us to treat the embedding solution as an infinite reservoir of (monovalent) salt of concentration $n_0^+ = n_0^- = n_0 =$ constant. Under these assumptions, the total volume of the solution is irrelevant for phase transitions involving the condensed phases.

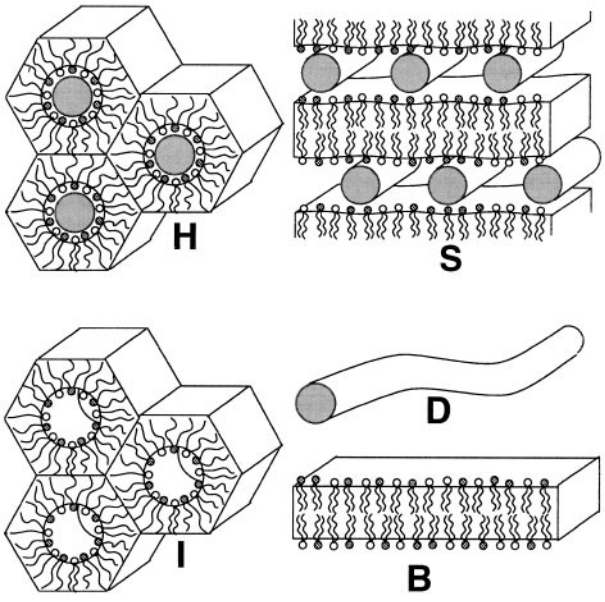

FIGURE 1 Schematic illustration of the five macroscopic phases included in our theoretical scheme. The phases denoted by H and S are the H_{II}^C and L_α^C complex structures, respectively. The symbols I and B mark the H_{II} and L_α phases, respectively. D represents uncomplexed DNA. The shaded regions correspond to the DNA cross sectional area. The lipid layers are mixed, consisting of cationic and uncharged (helper) lipids.

At a given temperature T and salt concentration n_0, our three-component system (DNA, CL, HL) is specified by two composition variables,

$$m = \frac{N^+}{N^+ + N^0}, \qquad \rho = \frac{N^+}{M}. \tag{1}$$

Here, m is the mole fraction of the cationic lipid in the original lipid mixture, and ρ is the ratio between the total number of cationic and DNA charges in the system. Equivalently, because all lipids, whether in pure lipid phases or DNA–lipid complexes, are organized in monolayers, we can regard ρ as the ratio between positive and negative macroion charges in the solution (to distinguish from the mobile counterion charges).

The total free energy of the three-component system $F = F(N^+, N^0, M; n_0, T)$ is a sum of terms corresponding to the various phases. Each term involves several thermodynamic and structural degrees of freedom. The phase diagram of the system is determined by minimizing F with respect to these variables subject to material conservation conditions. In the two following subsections, we first define the relevant degrees of freedom corresponding to the various phases, and then describe our model for calculating the free energy components of each phase. We end this section with a brief discussion of the approximations and assumptions used in our theoretical model and their possible influence on our conclusions.

Phases

DNA

We treat the double-stranded DNA as an infinitely long and straight rod, ignoring end effects as well as translational and conformational entropy contributions to its free energy. More specifically, the DNA is treated as a rigid rod of radius $R_D = 10$ Å, (corresponding to the surface of B-DNA), with uniform surface charge density $\sigma_D = -e/2\pi R_D b$; $b = 1.7$ Å is the mean distance between charges (projected) on the DNA axis. (We postpone discussing these, and other, approximations to the end of this section.) We shall assume that the dielectric constant inside the DNA rod is vanishingly small compared to that of the aqueous phase. The free energy of the DNA phase (D in the phase diagrams) is entirely due to the electrostatic charging energy of the rod in the given salt solution. Its contribution to F is $F_D = bM_D\hat{f}_D$ where bM_D is the length of uncomplexed DNA in solution

and $\hat{f}_D$ is its charging free energy per unit length, (hereafter 1 Å). Note that, for given n_0 and T, $\hat{f}_D$ is constant.

Lipid bilayer

We use N_B^+ and N_B^0 to denote the number of CL and HL molecules in the bilayer phase, respectively. (Consistent with the common nomenclature, we shall use L_α [= lamellar] to denote the bilayer phase. In the phase diagrams, and as subscripts, we replace L_α by B.) The two lipid species are assumed to be uniformly mixed, forming an ideal two-dimensional (2D) fluid mixture. We use the same cross-sectional area per molecule, $a = 70$ Å^2, for both the CL and HL molecules.

The total number of molecules in the L_α phase is $N_B = N_B^+ + N_B^0$. Its composition, specified by $\phi_B = N_B^+/N_B$, is the only relevant intensive variable of the bilayer; ϕ_B determines the surface charge density, $\sigma_B = e\phi_B/a$, and the elastic properties of a given lipid mixture. The contribution of the bilayer phase to the total free energy F is $F_B = N_B f_B(\phi_B)$, with $f_B(\phi_B)$ denoting the free energy per lipid molecule in a bilayer of composition ϕ_B; f_B involves electrostatic (charging), elastic and mixing terms, all depending on ϕ_B. The hydrophobic lipid chain regions in the bilayer phase and in all other phases will be treated as a medium of zero dielectric constant.

Inverse-hexagonal phase

We use N_I^+ and N_I^0 to denote the number of CL and HL molecules in the inverse-hexagonal lipid phase, H_{II} (for notational brevity we use I = inverse, rather than H_{II} as the subscript denoting this phase). The total number of lipids in this phase is $N_I = N_I^+ + N_I^0$, and its lipid composition is $\phi_I = N_I^+/N_I$. We assume that the radius of the water tubes, $R_I = 13$ Å, and the area per lipid molecule $a = 70$ Å^2 are constant, independent of ϕ_I, and hence of the cationic surface charge density. Note that we use the same area per molecule for both the planar and the inverse-hexagonal phases. This is a reasonable approximation provided this area, a, is measured at the so-called "pivotal surface," as discussed in more detail later in this section.

For the cylindrical symmetry of the H_{II} phase, the area per headgroup, a_{hg}, and the area at the pivotal surface (typically located just inside the hydrophobic region) a are related by,

$$a_{hg} = a(1 + hc_I) = aR_I/(R_I + h), \tag{2}$$

with h denoting the distance of the headgroup surface from the pivotal surface and $c_I = -1/(R_I + h)$ is the monolayer curvature at this surface. We adopt here the convention that the curvature of the inverse hexagonal phase is negative. In the calculations presented in the next section, we shall use $h = 6$ Å, which, for $R_I = 13$ Å and $a = 70$ Å^2, implies $a_{hg} = 47.9$ Å^2.

Subject to the assumptions above the free energy of the H_{II} phase, $F_I = N_I f_I(\phi_I)$, depends on one intensive variable, ϕ_I. Like in the bilayer phase, the free energy per molecule, $f_I(\phi_I)$, is a sum of electrostatic, elastic, and mixing contributions.

Lamellar complexes

The L_α^C (or S = sandwich) phase is an ordered smectic-like array, as schematically illustrated in Fig. 1. It is composed of N_S^+ cationic lipids, N_S^0 helper lipids, and M_S DNA charges. The lipid composition is specified by $\phi_S = N_S^+/N_S$; $N_S = N_S^+ + N_S^0$. The L_α^C phase is a periodic structure in the plane (x, y) perpendicular to the DNA axis (z), translationally invariant along z. Assuming that the lipid bilayers are perfectly planar, the structure of this phase is specified by the DNA–DNA repeat distance, d, the distance between apposed lipid surfaces, l, and the thickness of the lipid bilayers, w. Because the dielectric constant within the hydrophobic region is set equal to zero, w does not enter our model for the electrostatic energy. The bilayer thickness affects the bilayer bending rigidity, yet this is already accounted for by our choice of the bending constant, k, (see below). Also, both experimentally (Rädler et al., 1997) and theoretically (Harries et al., 1998), it was shown that the thickness of the water gap, l, is essentially independent of ϕ_S, for all relevant compositions. Consistent with this finding we shall use $l = 2(R_D + \delta) = 26$ Å with $\delta = 3$ Å denoting the thickness of the thin hydration layer separating the lipid and DNA charges.

The free energy of the L_α^C phase, F_S, depends on two independent intensive variables; e.g., the mole fraction of charged lipid, ϕ_S, and the positive/negative charge ratio $\rho_S = N_S^+/M_S$. These composition variables also determine the only structural variable of the L_α^C phase, d; namely, $d = N_S a/2M_S b = (a/2b)\rho_S/\phi_S$. We can thus write $F_S = N_S f_S(d, \phi_S) = bM_S \hat{f}_S(d, \phi_S)$, where $f_S(d, \phi_S)$ is the free energy per lipid in the L_α^C phase. In the second equality, $\hat{f}_S$ is the free energy of the L_α^C phase per unit length of DNA. We shall also refer to $\hat{f}_S$ as the free energy per unit cell of the complex.

Hexagonal complexes

The H_{II}^C (or H = honeycomb) phase consists of N_H^+ cationic lipids, N_H^0 helper lipids, and M_H DNA charges. Its lipid composition is $\phi_H = N_H^+/N_H$ with $N_H = N_H^+ + N_H^0$ denoting the number of lipids in the hexagonal complex. The radius of curvature of the (strongly curved) lipid headgroup surface in the H_{II}^C phase, R_H, must be larger than the radius R_D of the DNA strands intercalated within the cylindrical water tubes. We thus set $R_H = R_D + \delta = 13$ Å, with $\delta = 3$ Å

denoting the thickness of the water layer intervening between the DNA and lipid charges. This choice is based on experimental observations (Koltover et al., 1998). Note also that small δ ensures (at isoelectricity) efficient electrostatic charge balance (May and Ben-Shaul, 1997). Furthermore, as will be discussed in the next subsection, large δ, and hence large R_H, implies a high energetic penalty associated with the unfavorable stretching of lipid tails toward the interstitial axes within the hydrophobic core of the hexagonal phase (Seddon and Templer, 1995; Kirk et al., 1984; Gawrisch et al., 1992; Leikin et al., 1996; Kozlov et al., 1994). Finally, note that, to simplify the calculations, we have set $R_I = R_H$. Thus, the areas per molecule in the pivotal and headgroup surfaces in the H_{II}^C complex are related by Eq. 2.

Assuming R_H = constant, the H_{II}^C phase is characterized by a single intensive variable: ϕ_H. The free energy of this phase is then $F_H = N_H f_H(\phi_H) = bM_H\hat{f}_H(\phi_H)$, where f_H is the free energy per lipid molecule, and $\hat{f}_H$ is the free energy per unit length of DNA. Note that $N_H/M_H = 2\pi R_H b/a_{hg} = 2\pi(R_D + \delta + h)b/a$, implying $\hat{f}_H = [2\pi(R_D + \delta + h)/a]f_H$.

Degrees of freedom

The DNA/CL/HL mixture can exhibit a variety of phase equilibria. One way to map the phase diagram of this system is to consider all possible two- and three-phase equilibria, solve the relevant coexistence equations, and identify the phase boundaries by matching the chemical potentials of the pertaining components. We adopt here an alternative, computationally more efficient, route. Namely, we express the total free energy of the three-component mixture, F, as a sum of contributions representing all possible phases and minimize it with respect to all relevant variables. For every given lipid/DNA mixture the minimization yields the number and identity of the coexisting phases, their relative proportions, and their compositional and structural characteristics.

Explicitly, our free energy functional involves eleven concentration variables: four N_i^+ (i = B, I, S, H), four N_i^0, and three M_i (i = D, S, H). All quantities appearing in F,

$$F = N_H f_H(\phi_H) + N_S f_S(d, \phi_S) + N_B f_B(\phi_B) + N_I f_I(\phi_I) + bM_D\hat{f}_D, \quad (3)$$

are functions of these variables, e.g., $N_H = N_H^+ + N_H^0$, $\phi_H = N_H^+/N_H$, etc. However, not all variables are independent. Furthermore, according to the phase rule, there can be no more than three coexisting phases, implying that (following the minimization of F for a given mixture) some of the concentrations must vanish.

For a given mixture, characterized by the total numbers of molecules, M, N^+, and N^0, three of the eleven variables are eliminated by the material conservation conditions,

$$\begin{aligned} N^+ &= N_B^+ + N_I^+ + N_S^+ + N_H^+, \\ N^0 &= N_B^0 + N_I^0 + N_S^0 + N_H^0, \\ M &= M_D + M_S + M_H. \end{aligned} \quad (4)$$

Yet another variable can be counted out because of the structural-compositional constraint imposed on the H_{II}^C phase,

$$N_H = [2\pi(R_D + \delta + h)b/a]M_H. \quad (5)$$

Subject to these conditions, F is now a function of seven independent variables. The thermodynamic state of a given lipid/DNA mixture (M, N^+, N^0) is determined by the global minimum of F in the multidimensional space defined by the seven composition variables. Note that specifying M, N^+, and N^0 is equivalent to specifying ρ and m, (see Eq. 1), and one extensive variable that is irrelevant for determining the phase behavior of the mixture. Thus, the phase diagrams presented in the next section will be described in the ρ, m plane.

As a convenient reference point for calculating F, we choose the state where all lipids reside in a planar bilayer and all DNA is uncomplexed. Relative to this state, the free energy of the system is given by

$$\Delta F = F - Nf_B(m) - bM\hat{f}_D. \quad (6)$$

When all lipids and DNA are associated in one phase, e.g., the lamellar complex, this free energy change may be regarded as the formation free energy of this phase.

Free energies

In this section, we describe the various contributions to the free energy of the different phases, and their dependence on the relevant chemical compositions. In fact, for all phases except the naked DNA (D), the free energy is of the form

$$f_\alpha = f_\alpha^{es} + f_\alpha^{el} + f_\alpha^{mix} \quad (\alpha = S, H, B, I), \quad (7)$$

where the three terms on the right-hand side of this equation represent the electrostatic (charging) free energy, the elastic curvature energy, and the 2D mixing entropy of the lipid layers, respectively. In the following, we briefly discuss each of these contributions and its specific form in a given phase.

Electrostatics

The gain in electrostatic free energy is the driving force for the mutual condensation of DNA and cationic vesicles to form an ordered, composite phase. The major contribution to this free energy change is the entropy gain associated with the release of partially bound counterions into the bulk

solution (Harries et al., 1998; Bruinsma, 1998; Wagner et al., 2000). Before the association of the oppositely charged macroions (DNA and cationic lipid vesicles), each macroion is surrounded by a diffuse layer of partially bound counterions. In the condensed CL-DNA phase, most of these counterions are no longer needed for charge neutrality and can thus be released (Wagner et al., 2000).

The electrostatic free energy depends on the surface charge densities of the separated macroions, the structure and composition of the condensed phases, and the salt concentration in solution. The electrostatic free energies of the various structures are calculated based on the nonlinear PB equation. Although the PB approach involves some inherent approximations (see below), it was shown to predict adequately the principal structural and phase characteristics of both the H_{II}^{C} phase (May and Ben-Shaul, 1997) and the L_{α}^{C} phase (Harries et al., 1998). Here, we use the same algorithms for calculating the electrostatic free energy components of the many-phase system. All our PB calculations apply to symmetric 1:1 electrolyte solutions.

According to PB theory, the electrostatic (charging) free energy of any surface, or group of surfaces, in solution can be expressed in the form (Verwey and Overbeek, 1948),

$$F^{es} = \frac{1}{2}\int_S \sigma\Phi \, ds + k_B T n_0 \int_V [\Psi \sinh \Psi - 2\cosh \Psi + 2] \, dv. \tag{8}$$

The first integral extends over all the charged surfaces, S, where σ denotes the local surface charge density and Φ is the corresponding electrostatic potential. The second integration is over the volume, V, of the electrolyte solution; $\Psi = e\Phi/k_B T$ is the reduced electrostatic potential. In writing Eq. 8, it is assumed that the dielectric constant inside the DNA and lipid membrane is vanishingly small compared to the aqueous solution.

To obtain Ψ, we solve the PB equation,

$$\nabla^2\Psi = \kappa^2 \sinh \Psi, \tag{9}$$

with $l_D = 1/\kappa$ denoting the Debye screening length; $\kappa^2 = 8\pi l_B n_0$ where $l_B = e^2/4\pi\epsilon_0\epsilon_r k_B T$ is the Bjerrum length; ϵ_0 is the permittivity of vacuum and $\epsilon_r = 78$ the dielectric constant of the aqueous phase. In water at room temperature, $l_B = 7.14$ Å. In all calculations, we have used $n_0 = n_0^+ = n_0^- = 4$ mM for the salt concentration, corresponding to $l_D = 50$ Å.

The solutions of the PB equation depend on the specific boundary conditions for the system considered. We shall now briefly describe the boundary conditions appropriate for the five structures illustrated in Fig. 1, and the corresponding free energies. Additional details are given elsewhere (Harries et al., 1998; May and Ben-Shaul, 1997).

L_{α}. The existence of a low dielectric hydrophobic region between the two bilayer surfaces allows treating them as separate, electrostatically decoupled, cationic surfaces. The PB equation of a charged planar surface is one-dimensional: $d^2\Psi/dz^2 = \kappa^2 \sinh \Psi$, with z denoting the distance from the charged surface. The boundary conditions are $\Psi' = d\Psi/dz = 0$ at $z \to \infty$ and $\Psi' = -4\pi\phi_B l_B/a$ at the charged surface. Upon substituting the solution for Ψ into Eq. 8, one obtains the well-known expression for the free energy per molecule in terms of $p = 2\phi_B \pi l_B l_D/a$ and $q^2 = p^2 + 1$ (Lekkerkerker, 1989),

$$\frac{f_B^{es}(\phi_B)}{k_B T} = 2\phi_B\left[\frac{1-q}{p} + \ln(p+q)\right]. \tag{10}$$

Unfortunately, this is the only geometry for which the PB equation can be solved analytically.

H_{II}, H_{II}^{C}, D. In all these three geometries, the charged surfaces are cylindrically symmetric. Thus, the PB equation is again one-dimensional, involving only the radial coordinate r. Using Ψ' for $d\Psi/dr$, etc., the PB equation reads $\Psi'' + \Psi'/r = \kappa^2 \sinh \Psi$.

The boundary conditions for an isolated DNA rod (D phase) are $\Psi' = 0$ at $r = \infty$, and $\Psi'(R_D) = 2l_B/R_D b$ at the surface of the rod.

For the H_{II} phase the PB equation is solved within the inner aqueous cylinders. The boundary conditions are $\Psi'(0) = 0$ and $\Psi'(R_I) = 4\pi\phi_I l_B/a_{hg}$; $R_I = R_D + \delta$.

Intercalating the DNA rods within the water tubes of the H_{II} phase, we obtain the geometry of the H_{II}^{C} phase. The electrostatic problem here consists of two concentric, oppositely charged, surfaces. The PB equation is solved for the aqueous region between the two surfaces, $R_D \le r \le R_H$. The boundary conditions are $\Psi'(R_D) = 2l_B/R_D b$ at the DNA surface, and $\Psi'(R_H) = 4\pi\phi_H l_B/a_{hg}$ at the lipid surface. Recall that we use $R_H = R_I = R_D + \delta$.

The PB equation for this geometry has been solved numerically for different values of the surface charge densities and the radius of the outer (lipid) cylinder. These solutions reveal that the electrostatic free energy is always minimal at, or very near, the isoelectric point, where the surface charges are equal in magnitude and opposite in sign. At this point, for surface spacings δ, typical of the H_{II}^{C} phase (several Å), most counterions in excess of the bulk concentration are released from the cylindrical aqueous gap into the bulk solution, resulting in maximal entropy gain of these mobile ions. Because there are very few counterions in the gap, the two concentric surfaces can be treated as constituting a cylindrical capacitor (May and Ben-Shaul, 1997). In the next section, we show that, at the isoelectric point, this model yields very good agreement with the numerical solutions of the PB equation. Away from the isoelectric point

we use the PB equation to approximate the increase in the electrostatic free energy, as discussed in the next section.

L_α^C. The PB equation for the unit cell of the L_α^C phase is 2D, (because the system is translationally invariant along the DNA-axis direction). The boundary conditions here are more intricate and add a nontrivial aspect to the PB theory. Namely, because the DNA rods are nearly touching the lipid monolayers, they polarize the 2D lipid mixture, attempting to concentrate the right amount of CL molecules in their vicinity. This polarization is partly opposed by the entropic penalty associated with the demixing of the two lipid species. The actual lipid charge distribution is determined by the balance between these opposing forces, as dictated by minimizing the total (electrostatic and mixing) free energy of the complex. This minimization results in a locally varying boundary condition at the lipid layers, which must be solved self-consistently with the PB equation. More details are given elsewhere (Harries et al., 1998).

Elastic energy

Lipid bilayers and monolayers are elastic membranes, which, at a certain free energy cost, can either be stretched or bent (or both) with respect to their equilibrium state (Helfrich, 1973). The energy penalty associated with curvature deformations is generally much smaller than that involved in area changes. For this reason, we can treat the membranes as laterally incompressible. In contrast, we must account for the ability of cationic membranes to undergo curvature deformations under the strong electrostatic forces exerted by the highly charged and strongly curved DNA strands. Thus, in the presence of DNA in its immediate vicinity, a planar cationic lipid bilayer may re-assemble into inverse-hexagonal layers, enveloping the DNA strands. This rearrangement is most likely to take place when the bilayer is composed of monolayers characterized by negative spontaneous curvature. When this propensity is strong enough, as is the case with pure DOPE systems, the inverse-hexagonal phase will appear even in the absence of DNA (Gawrisch et al., 1992; Leikin et al., 1996; Chen and Rand, 1998). Otherwise, i.e., if the spontaneous curvature is not sufficiently negative, the monolayers assemble into a planar bilayer, paying the necessary but tolerable curvature frustration energy toll.

In mixed lipid layers, the spontaneous curvature is a function of composition. For example, in the CL/HL mixture DOTAP/DOPE, the spontaneous curvature becomes increasingly negative as the mole fraction of the helper lipid increases. Without DNA the bilayer will destabilize at a certain mole fraction of the helper lipid, undergoing a phase transition from the planar to the inverse hexagonal geometry. The addition of DNA to the mixture can promote the transition to take place at a considerably lower concentration of the helper lipid. These effects play a crucial role in determining the phase behavior of CL/HL/DNA system. We account for them using a simple model for the bending rigidity of mixed lipid layers.

The elastic energy of the lipid monolayers constituting the four lipid-containing phases illustrated in Fig. 1 will be expressed in the form,

$$f^{el}(c, \phi) = a(k/2)(c - c_0(\phi))^2 + f_v. \qquad (11)$$

The first term in this equation represents the familiar elastic deformation energy, per molecule, in a cylindrically bent lipid monolayer (Helfrich, 1973). Here, k is the bending modulus, c_0 is the spontaneous curvature of the monolayer, c is the actual curvature, and a the area per molecule. We use this expression for both the planar and inverse-hexagonal geometries, assuming that k, a, and c_0 are the same for both curvatures. The second term corrects for the fact that, in the inverse-hexagonal symmetry, not all molecules experience the same deformation. Those molecules whose hydrophobic tails point toward the hexagonal interstices (or voids) of the hydrophobic core are more extensively stretched than those directed toward neighboring water tubes. Because not all lipid tails are equally stretched, some of them are necessarily "frustrated," resulting in an average free energy penalty of f_v per molecule (see e.g., Kirk et al., 1984; Seddon and Templer, 1995). It should be noted that a, c, c_0, and k are measured with respect to the pivotal surface where, upon cylindrical deformations, the area per molecule stays constant (see e.g., Gawrisch et al., 1992; Leikin et al., 1996; Kozlov et al., 1994). For laterally incompressible lipid monolayers, as we assume to be the case here, the pivotal surface coincides with the neutral surface, where area and curvature deformations are, by definition, decoupled. Typically, the pivotal surface lies inside the hydrophobic region, close to the hydrocarbon–water interface (Leikin et al., 1996; Kozlov et al., 1994).

In general, both k and c_0 depend of the lipid composition ϕ. In the calculations presented in the next section, we shall assume that k is independent of ϕ, as is often the case for lipid molecules of similar chain length. For the dependence of the spontaneous curvature on ϕ, we shall adopt the simple but adequate linear interpolation formula (May and Ben-Shaul, 1995; Andelman et al., 1994),

$$c_0(\phi) = c_0^h + \phi(c_0^c - c_0^h), \qquad (12)$$

where c_0^c and c_0^h are the spontaneous curvatures of the cationic and helper lipids, respectively.

Eqs. 11 and 12 will be used for all four lipid-containing phases considered in this work. Clearly, for the two lamellar phases $f_v = 0$. The curvatures of the lipid-containing phases are $c = c_B = c_S = 0$, $c_I = c_H = -1/(R_D + \delta + h) = -1/19$ Å (recall $R_D = 10$ Å, $\delta = 3$ Å, and $h = 6$ Å). In the calculations reported in the next section, we shall consider several different lipid mixtures, corresponding to different sets of the elastic constants k, c_0^h, and f_v.

Finally, it should be noted that the bending rigidity of charged lipid layers is a sum of contributions of different origins, including entropic (conformational) repulsions between the hydrocarbon tails as well as steric and electrostatic repulsions between headgroups. In Eq. 11, we include all contributions to the elastic energy except the electrostatic one. When electrostatic-curvature effects are small, they can be accounted for through an additional contribution to the bending rigidity k, i.e., to the first term in Eq. 11. Usually, this contribution is derived from the second-order term in the curvature expansion of the PB electrostatic energy (Lekkerkerker, 1989). However, the surfaces in the H_{II} and H_{II}^C phases are not only highly curved but also closed. Furthermore, for the same lipid mixture, the cationic charge densities in the hexagonal phases are different from those in the planar phases (May, 1996). Thus, instead of treating the changes in electrostatic energy based on low-order curvature expansions, we use the full nonlinear PB solution for all geometries.

Mixing entropy

As in other phase separation phenomena, when two or more lipid-containing phases coexist in solution, their CL/HL compositions are generally different, implying different mixing entropies. Following previous studies (May and Ben-Shaul, 1997; Harries et al., 1998), we shall assume that the monolayers in the L_α, H_{II}, and H_{II}^C phases are ideal 2D mixtures. Their mixing free energy is thus given by

$$f^{mix}/k_BT = \phi \ln \phi + (1 - \phi)\ln(1 - \phi). \qquad (13)$$

The presence of DNA strands in the L_α^C phase induces a nonuniform distribution of the two lipid components. The deviations from ideal mixing in this phase are taken into account in the electrostatic free energy, f_S^{es}. For the uniform mixing entropy of this phase, we use Eq. 13.

Molecular free energies

Adding the electrostatic, elastic, and mixing contributions as in Eq. 7, the free energies per lipid molecule in the four lipid-containing phases are given by:

$$\begin{aligned} f_H(\phi_H) &= f^{el}(c_H, \phi_H) + f_H^{es}(\phi_H) + f^{mix}(\phi_H), \\ f_S(d, \phi_S) &= f^{el}(0, \phi_S) + f_S^{es}(d, \phi_S) + f^{mix}(\phi_S), \\ f_B(\phi_B) &= f^{el}(0, \phi_B) + f_B^{es}(\phi_B) + f^{mix}(\phi_B), \\ f_I(\phi_I) &= f^{el}(c_I, \phi_I) + f_I^{es}(\phi_I) + f^{mix}(\phi_I). \end{aligned} \qquad (14)$$

Using these expressions in Eqs. 3 and 6, we can calculate the formation free energy, ΔF, for any specific partitioning of the DNA and lipids (both cationic and uncharged) among the different phases. Minimizing ΔF with respect to the seven concentration variables in this expression, we obtain the number, nature, and compositions of the phases corresponding to a system with given ρ and m.

Approximations of the model

The systems modeled in the present study are very complex, both with respect to the structure of the phases considered and the variety of contributions to their free energies. Thus, the theoretical analysis of their phase behavior necessarily involves quite a few assumptions and approximations. Let us briefly review the most important approximations and their possible consequences.

The model involves several simplifying assumptions pertaining to the structure of the phases considered. For instance, by treating a double-stranded DNA as a rigid cylindrical rod with negative charges uniformly distributed over its surface, we ignore the groove structure and the discrete distribution of phosphate charges. Although this picture provides a reasonable approximation for the electrical potential several angstroms away from the charged surface, (Wagner et al., 1997), it may quantitatively fail at the immediate vicinity of the surface. This, in turn, may affect our numerical estimates of the electrostatic energies of the DNA-lipid complexes where the DNA and lipid charges are nearly in contact. Ignoring the molecular structure of water, the finite size of the counterions, and using the continuous, mean-field, PB approach to calculate the electrostatic energies of these complexes are additional approximations. Still, using this approach to calculate the phase structure and phase behavior of lamellar complexes, we obtained good agreement with experiment, (Rädler et al., 1997), both with respect to the variation of the DNA–DNA spacing, d, as a function of the lipid/DNA ratio, ρ, and the dependence of the phase boundaries on the CL/HL lipid composition. This agreement may be attributed to the fact that some features of the model are robust, e.g., the occurrence of the free energy minimum at the isoelectric point.

Here, the same structural and electrostatic free energy assumptions are used consistently to analyze phase transitions between phases of markedly different symmetries, e.g., the H_{II}^C and L_α^C phases. Even though we use approximate theories, the resulting phase behaviors are quite complex, and strongly dependent on the elastic and electrostatic properties of the lipid mixture. Although our theoretical model does not include all possible free energy contributions, it certainly captures the chief features of the relevant phase diagrams. It may fail to predict the exact locations of phase boundaries, but not the nature of the phases and phase transitions observed, which is our main goal in this work.

One can also argue, for instance, that PB theory is inappropriate for considering the counterion distributions within the narrow aqueous confines of the lamellar or hexagonal complexes. Yet, our calculations reveal that, whenever these structures appear in solution, their net fixed charge is generally very small, i.e., the complexes are nearly isoelec-

tric. Consequently, the counterion concentration within the narrow aqeuoes regions is typically small, in which case PB theory provides an adequate approximation, (subject, of course, to the approximations used to describe the structure of the charged surfaces).

Our model involves various other approximations. For example, we ignore conformational entropy contributions associated with the (very small) flexibility of double-stranded DNA or the curvature fluctuations of the lipid layers. Yet, these contributions are negligible compared to the electrostatic or elastic free energy differences between the various phases. (For instance, the conformational entropy of DNA is of order 1 k_BT per DNA persistence length ($l_P \approx 500$ Å), whereas the electrostatic and elastic energies are of order 1 k_BT per 1 Å).

Assuming an ideal mixing of the lipids in the various phases (except the L_α^c) and our simple model for the spontaneous curvature of the mixed lipid layers, represent additional approximations. In contrast, it should be remembered that uncertainties are also involved in the values of the elastic constants of even the best studied lipid systems. Still, it is clear that lipids preferring the hexagonal symmetry must have very different spontaneous curvatures from those that self-assemble into lipid bilayers. The model calculations presented in the next section aim to account for qualitative differences on this level, rather than those resulting from small variations of the elastic constants.

RESULTS AND DISCUSSION

The most interesting and relevant phases in lipid–DNA mixtures are, of course, the lipoplexes. Our model accounts for the two most important structures, namely, the H_{II}^C and L_α^C phases. In both phases, the DNA and lipid layers are tightly associated, yet the complexation geometries are qualitatively different. These differences imply different electrostatic stabilization energies and different dependencies on the elastic properties of the lipid layers and their composition.

The goal of the forthcoming analysis is to provide a theoretical scheme for predicting the conditions favoring one lipoplex phase over the other or, possibly, the coexistence of both structures. The term "conditions" refers here to the elastic properties of the lipid monolayers on the one hand, and the relative amounts of HL, CL, and DNA in solution, i.e., ρ and m, on the other.

As we shall see below, the phase diagrams of CL/HL/DNA mixtures may exhibit rather complex behaviors, involving a variety of phase transitions and coexistence regimes. To assist the interpretation of these phase diagrams, we begin the discussion with two preparatory subsections. In the first, we compare the electrostatic free energies of the two complex phases as a function of lipid composition and lipid/DNA ratio. The second subsection is concerned with the effects of electrostatic interactions on the relative stabilities of the pure lipid phases, L_α and H_{II}.

All the calculations presented below were carried out for $n_0 = 4$ mM, ($l_D = 50$ Å). Similar phase behaviors correspond to lower salt concentrations. Significant differences are expected only at very high salt contents, that is, when the Debye length becomes considerably smaller than the dimension of a typical lipoplex unit cell. In this limit, however, the complexes become unstable.

Electrostatics of the H_{II}^C and L_α^C phases

In our phase diagram calculations, the radius of the lipid headgroup surfaces in the H_{II}^C phase is kept fixed at $R_H = R_D + \delta = 13$ Å. It is instructive, however, to examine how the electrostatic free energy of this structure varies with δ and ϕ_H. In Fig. 2, the electrostatic free energy per hexagonal unit cell, $\hat{f}_H^{es}$, is shown as a function of ϕ_H for four values of the water gap thickness; $\delta = 0.5$, 3.0, 8.5, and 15.0 Å. (The lowest value of δ is unrealistic, because we must allow for at least a minimal water layer, which we set equal to $\delta = 3$ Å. It is shown only for comparison.) Note that

$$\hat{f}_H^{es}(\phi_H) = 2\pi[(R_D + \delta + h)/a] f_H^{es}(\phi_H), \qquad (15)$$

where f_H^{es} is the electrostatic energy per lipid molecule in the H_{II}^C phase. For $R_D + \delta + h = 19$ Å and $a = 70$ Å^2, we have $\hat{f}_H^{es}/f_H^{es} \simeq 1.7$ Å^{-1}.

For all δ, we find that the free energy $\hat{f}_H^{es}(\phi_H)$ is minimal at, or very near, the isoelectric point. At this point, ϕ_H is given by

$$\phi_H^* = \frac{a}{2\pi(R_D + \delta + h)b}, \qquad (16)$$

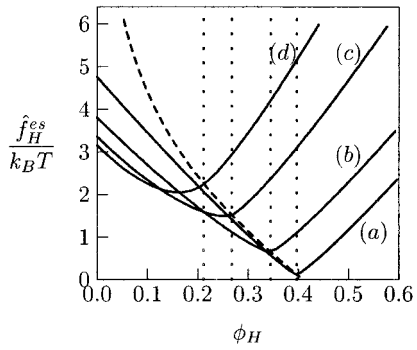

FIGURE 2 The electrostatic free energy, $\hat{f}_H^{es}$, of the H_{II}^C complex per hexagonal unit cell (of length 1 Å) for (*a*), $\delta = 0.5$ Å; (*b*), $\delta = 3.0$ Å; (*c*), $\delta = 8.5$ Å; and (*d*), $\delta = 15.0$ Å. The dotted lines indicate the compositions, ϕ_H^*, for which the H_{II}^C structure is isoelectrical. The dashed curve corresponds to the free energy, $\hat{f}^{cap}(\phi_H = \phi_H^*)$, according to the capacitor model, as given in Eq. 17.

as marked by the vertical dotted lines in Fig. 2. The minima of $\hat{f}_H^{es}$ are more pronounced and occur closer to the isoelectric point for the smaller values of δ.

The dashed curve in Fig. 2 denotes the electrostatic energy according to the capacitor model mentioned in the previous section. This is the free energy of a concentric cylindrical capacitor, composed of an inner surface of radius $R_D = 10$ Å and an outer surface of radius $R_H = R_D + \delta$, with water as the dielectric medium. The charge densities on these two surfaces are $-e/2\pi bR_D$ and $e\phi_H/2\pi b(R_D + \delta)$, respectively. The charging energy per 1 Å of this capacitor is

$$\frac{\hat{f}_H^{cap}}{k_BT} = \frac{l_B}{b^2}\ln\frac{R_D + \delta}{R_D}, \tag{17}$$

with $\delta = a/2\pi b\phi_H - (R_D + h)$.

For $\delta \ll l_D$ (recall $l_D = 50$ Å), the minimum in the PB free energy exactly coincides with the simple capacitor model (*curves a* and *b* in Fig. 2), indicating that the surface charges are not screened by counterions. Namely, all the excess (diffuse layer) counterions have been expelled into the bulk solution. The capacitor model becomes less adequate as δ approaches l_D. Correspondingly, the minimum of $\hat{f}_H^{es}$ is shifted from ϕ_H^* to $\phi_H < \phi_H^*$, i.e., to a lower charge density of the outer surface, thus reducing the charging energy. The minimum of $\hat{f}_H^{es}$ increases, reflecting the less efficient charge neutralization associated with the increasing value of δ.

Unfortunately, the simple capacitor model is valid only at the isoelectric point. For $\phi_H \neq \phi_H^*$, we need the PB equation to calculate the electrostatic energy. When the surfaces are not equally charged, counterions must be present in the aqueous gap to ensure electrical neutrality. The reduced entropy of these counterions results in a repulsive interaction (disjoining pressure) between the apposed surfaces (Parsegian and Gingell, 1972). To a good approximation, this energy is equal to the capacitor energy plus the excess charging energy of the lipid surface (when $\phi_H > \phi_H^*$) or the DNA surface (when $\phi_H < \phi_H^*$), i.e., the charging energy of the relevant surface by the amount of charge $\phi_H - \phi_H^*$.

Hereafter, when referring to the H_{II}^C phase, we shall consistently use $\delta = R_H - R_D = 3$ Å. In addition to being the electrostatically most favorable configuration, this δ also corresponds to minimal chain stretching (frustration) energy in the inverse-hexagonal symmetry. The isoelectric point corresponding to $\delta = 3$ Å, $h = 6$ Å and $a = 70$ Å^2 occurs at $\phi_H = \phi_H^* = 0.345$.

Let us now compare the electrostatic energies per unit cell in the H_{II}^C and L_α^C complexes. In analogy to $\hat{f}_H^{es}$ in Eq. 15, we define $\hat{f}_S^{es}$ as the electrostatic free energy per 1 Å of the L_α^C unit cell,

$$\hat{f}_S^{es}(\phi_S) = (2d/a)f_S^{es}(\phi_S), \tag{18}$$

where $2d/a = N_S/(bM_S) = \rho_S/b\phi_S$.

In Fig. 3, we show $\hat{f}_S^{es}$ as a function of the fraction of charged lipid in the complex, ϕ_S, for several values of the DNA–DNA spacing d (Harries et al., 1998). Also shown, (*broken curve*), is the electrostatic free energy of the H_{II}^C phase for $\delta = 3$ Å, (*curve b* in Fig. 2). The curves marked *a–d* in Fig. 3 correspond to lamellar complexes containing exactly the same number of lipids per unit cell as those marked *a–d*, respectively, in Fig. 2, which describes the hexagonal complexes.

As for the H_{II}^C phase, for all values of d, the minima of $\hat{f}_S^{es}$ occur at the isoelectric point ($\phi_S = \phi_S^* = a/2bd$) or its immediate vicinity. However, unlike in the H_{II}^C phase, where the minima vary markedly with the unit cell dimensions (i.e., δ), the minima of $\hat{f}_S^{es}$ are nearly equal for all d. The reason for that is the ability of the CL/HL lipid layers in the L_α^C complex to polarize their charge density (demix the lipid distribution) so as to achieve close contact with the DNA charges. The demixing entropy penalty associated with this charge modulation is very small compared to the gain in electrostatic energy.

Two important conclusions can be derived from the results shown in Fig. 3. First, the L_α^C complex can respond to changes in lipid composition by varying the DNA–DNA distance, maintaining its electrostatic energy close to its minimum. Second, the global minimum of the electrostatic free energy of the H_{II}^C phase is lower than that of the L_α^C phase. The difference is a direct consequence of the different complex geometries. In the H_{II}^C phase all lipid charges are close to the DNA charges. In contrast, in the L_α^C phase only a fraction of the cationic lipids are close to the DNA strands, the rest are necessarily farther away, contributing less efficiently to charge neutralization.

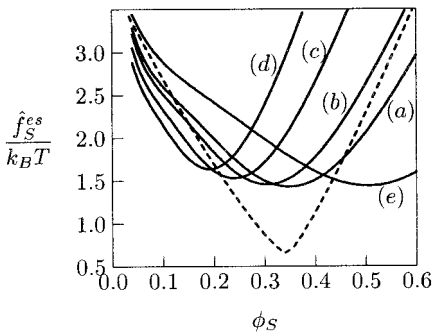

FIGURE 3 The electrostatic free energy of the L_α^C complex per unit cell (of length 1 Å), as a function of the CL mole fraction, ϕ_S. The solid curves correspond to five representative values of the DNA–DNA spacing: (*a*), $d = 51.8$ Å; (*b*), $d = 59.7$ Å; (*c*), $d = 77.0$ Å; (*d*), $d = 97.4$ Å; and (*e*), $d = 35.0$ Å. (The minimal value of d is $d = 2R_D + \delta = 23$ Å.) For comparison, we also show (*broken curve*) the electrostatic energy of the hexagonal complex, $\hat{f}_H^{es}(\phi_H)$, for $\delta = 3$ Å (curve (*b*) in Fig. 2). Note that a given d implies a given number of lipid molecules in the L_α^C complex. The solid curve (*b*) and the broken curve correspond to the same number of molecules (per unit DNA length) in the lamellar and hexagonal complexes, respectively.

From Fig. 3, it is also apparent that the electrostatic dominance of the H_{II}^{C} complex is limited to a finite range of compositions around its isoelectric point. Consider first the two curves marked *b* in Figs. 2 and 3, the former is shown again (*dashed curve*) in Fig. 3. Both curves correspond to the same number of lipids per unit cell. Thus, the difference between these two curves represents the free energy change associated with the complete transformation of an H_{II}^{C} unit cell into an L_{α}^{C} unit cell, containing the same number of lipids at the same composition, $\phi = \phi_H = \phi_S$. Comparing $\hat{f}_H^{es}$ with $\hat{f}_S^{es}$ we find that, electrostatically, this complete transition is favorable only for $\phi < 0.15$ (where *curve b* crosses the *broken line*). Recall, however, that the lamellar complexes can lower their free energy by adjusting their DNA–DNA spacing, and hence the number of lipid molecules in the unit cell. From Fig. 3, we conclude that, when this additional degree of freedom is taken into account (i.e., allowing the lamellar complex to shift from one *d* curve to another), the electrostatic preference of the hexagonal complex is limited to a considerably smaller range of lipid compositions. It should be noted, however, that these considerations ignore the important effects of membrane elasticity, which may either narrow or widen the regime over which one phase is more favorable than the other. They also ignore the important role of other phases in the system.

The $L_\alpha \rightarrow H_{II}$ transition

The phase behavior of lipid–DNA mixtures is strongly affected by the intrinsic propensity of the lipids to form, in the absence of DNA, a particular lipid phase. Lipoplexes are often prepared using helper lipids, such as DOPE, which, under physiological conditions, form the H_{II} phase, (Gawrisch et al., 1992; Leikin et al., 1996; Chen and Rand, 1998). These lipids are characterized by large, negative, spontaneous curvature. Adding to the mixture cationic lipids, or, more generally, lipids of small spontaneous curvature, will result in a first-order transition to the bilayer (L_α) phase at some well-defined composition.

The major characteristics of this transition are demonstrated in Fig. 4 for a CL/HL lipid mixture with the following elastic properties: $c_0^h = -1/25$ Å and $c_0^c = 0$ are the spontaneous curvatures of the helper and cationic lipids, respectively; $k = 10k_BT$ is the (monolayer) bending modulus of both lipid species, (the bilayer modulus is $2k$), $h = 6$ Å is the distance of the head group charges from the pivotal surface, and $f_v = 0.35k_BT$ is the stretching-frustration free energy of the inverse hexagonal phase. The elastic constants of the helper lipid correspond closely to those measured for DOPE and mixtures of DOPE with other lipids (Gawrisch et al., 1992; Leikin et al., 1996; Chen and Rand, 1998).

The figure shows the free energies of the two phases, f_B and f_I, as a function of the CL mole fraction. The lipid compositions at the transition are determined by the common tangent construction. The free energies were calculated

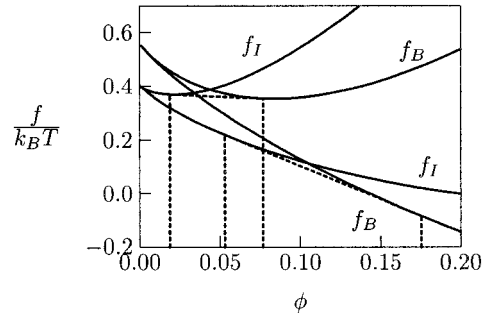

FIGURE 4 The free energies per lipid molecule, f_B and f_I in the lamellar (L_α) and inverse-hexagonal (H_{II}) phases, respectively, as a function of the lipid layer composition ϕ. The upper set of curves display the free energies per molecule as given in Eq. 14. In the lower set, the electrostatic contributions to f_B and f_I are omitted (that is, only the elastic, intersticial, and mixing contributions are included). The common tangent construction and the coexisting compositions, ϕ_H and ϕ_B, are marked by broken lines. The free energies were calculated for lipid layers with $k = 10k_BT$, $c_0^c = 0$, $c_0^h = -1/25$ Å, $f_v = 0.35$, $h = 6$ Å, and $l_D = 50$ Å.

using Eqs. 14. In the upper set of curves, the free energies of the two phases include all the relevant (i.e., electrostatic, elastic, and mixing) contributions. To emphasize the important role of the electrostatic free energy, we also show the free energies of these phases for a hypothetical, electrically neutral mixture with the same elastic properties. (In other words, in this calculation we have omitted f^{es} from f). From these calculations, it is apparent that the lipid charges enhance the $H_{II} \rightarrow L_\alpha$ transition. That is, the transitions sets in at a smaller value of ϕ. The origin of the electrostatic destabilization of the H_{II} phase is twofold. The mutual repulsion between cationic charges in the highly curved cylindrical tube and the strong confinement of the counterions within this tube.

Phase diagrams

In this section, we show three representative lipid-DNA phase diagrams, corresponding to CL/HL mixtures of qualitatively different elastic characteristics, i.e., different sets of k, c_0^c, and c_0^h. In the first system, both lipids prefer the planar monolayer curvature, ($c_0^h = c_0^c = 0$), and strongly resist curvature deformations (large k). The second system features the opposite limit, corresponding to very soft lipid monolayers, i.e., $k \simeq 0$. Besides the theoretical interest in this limit, it should be noted that very soft lipid layers ($k \leq 1k_BT$) can be prepared, for example, by adding short-chain alcohols to the lipid mixture (Safinya et al., 1989; Koltover et al., 1998; Szleifer et al., 1988). These added molecules may also enter the exagonal voids of the H_{II} phase and relieve the chain-stretching energy, (i.e., $f_v \simeq 0$). Clearly, for $k = 0$, the spontaneous curvature is irrelevant. Yet it should be noted that the phase behavior observed for $k = 0$ is essentially identical to the one calculated for $k \simeq 1k_BT$, $c_0^h = c_0^c = 0$, and $f_v = 0$. The third, perhaps the most

interesting, case describes a lipid mixture in which the cationic lipid still prefers the planar monolayer, ($c_0^c = 0$), but the helper lipid, such as DOPE, prefers the inverse-hexagonal geometry, ($c_0^h = -1/25\ \text{Å}^{-1}$). The phase behaviors of the three systems are qualitatively different in both the nature of the lipoplex phases that appear in solution and the complexity of the phase diagrams. They represent a rather wide range of experimentally interesting systems.

The phase diagrams will be presented in the ρ, m plane, the two (experimentally controllable) intensive variables specifying the overall chemical composition of the mixture. For each point in the ρ, m plane, the number, nature, proportions, and chemical compositions of the coexisting phases are determined by minimizing ΔF, (Eq. 6), with respect to the seven independent concentration variables defined by Eqs. 3, 4, and 5. The minimization is carried out numerically.

Rigid planar membranes

We first consider a lipid mixture where $c_0^h = c_0^c = 0$. For concreteness, we set $k = 10k_BT$, a rather common value for many lipid monolayers (Lipowsky and Sackmann, 1995). For these elastic constants, no hexagonal phases appear in our calculated phase diagram. Thus, the value of f_v, which further increases the free energy of these phases, is irrelevant. (In fact, for $c_0 \equiv 0$, $f_v = 0.35k_BT$ and $h = 6$ Å, identical phase diagrams are obtained for all monolayers with $k \geq 2.5k_BT$.) An experimental system with similar characteristics is the lipid mixture DOTAP/DOPC, which exhibits only lamellar lipid and lipoplex phases (Rädler et al., 1997, 1998). Lamellar complexes have also been observed using other lipid mixtures (Templeton et al., 1997; Battersby et al., 1998; Boukhnikachvili et al., 1997).

The phase diagram of the system considered is shown in Fig. 5. The structural and thermodynamic characteristics of this, relatively simple, mixture have been analyzed in detail, both experimentally (Rädler et al., 1997) and theoretically (Harries et al., 1998; Bruinsma, 1998). Below, we briefly outline those features of the phase diagram that are relevant for the forthcoming discussion.

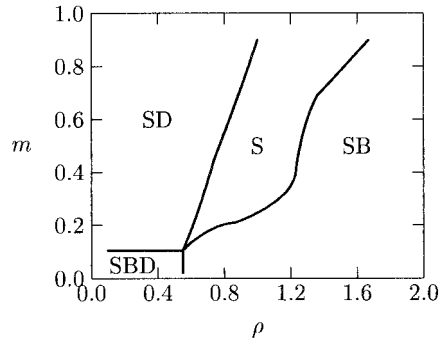

FIGURE 5 The phase diagram of a lipid–DNA mixture, for lipids that self-assemble into rigid planar membranes. The phase diagram was calculated for a membrane characterized by $k = 10k_BT$ and $c_0^h = c_0^c = 0$. The symbols S, B, and D denote, respectively, the L_α^C, L_α, and uncomplexed (naked) DNA phases. (See Fig. 1.)

Upon increasing ρ at constant m, the system evolves through three distinct stages, (except in the narrow regime $\rho \leq 0.1$). At low values of ρ, lamellar complexes coexist with an uncomplexed DNA phase. In this regime (SD in Fig. 5), the DNA–DNA distance is constant $d = d_1(m)$, ($d_1(m)$ increases with m). After ρ reaches a certain $\rho = \rho_1(m)$, all DNA and lipid become complexed and the system is monophasic. It remains monophasic as ρ increases until it reaches a second phase boundary, $\rho = \rho_2(m)$. Within the one-phase region, which (except for $\rho \leq 0.2$) includes the isoelectric point ($\rho = 1$), d increases linearly with ρ. When $\rho > \rho_2$, ($d > d_2(m)$), the system is again biphasic, with complexes coexisting with an excess bilayer phase. It is important to note that, in this (SB) regime, because of the possibility of lipid exchange, the lipid compositions in the complex and bilayer are different, both depending on ρ. Also, d slowly decreases with ρ. ϕ_S, ϕ_B, and d approach constant values at $\rho \gg 1$ (Harries et al., 1998).

The appearance of a small three-phase region in the left-bottom (small m, small ρ) corner of Fig. 5 is interesting theoretically, but of rather limited practical interest. This is because, at very low lipid charge densities, around $m \leq 0.15$, the electrostatic stabilization of the complexes is significantly reduced; the inter-bilayer spacing l begins to increase and the lamellar aggregates eventually disintegrate. Thus, our assumption that l is constant does not hold for very small values of m, certainly not below $m \approx 0.1$. Nevertheless, the existence of a small three-phase region cannot entirely be ruled out. Let us, therefore, briefly explain its thermodynamic-energetic origin.

When ρ is small, part of the DNA must be left uncomplexed. If all lipids were complexed, $\phi_S = m$ is necessarily small. Suppose momentarily that this is indeed the case, and that the complexes are essentially isoelectric. (Strongly overcharged, i.e., not isoelectric, complexes are less stable.) Because ϕ_S is small, d is large, implying poor DNA/lipid charge matching. The situation is improved if the cationic lipids concentrate in the vicinity of the DNA rods. Yet, this lipid segregation involves a nonzero demixing entropy penalty. As a result, the middle regions of the L_α^C complex unit cell remain weakly charged, implying an energy penalty due to the mutual repulsion of the two apposed monolayers in the complex. It is, in fact, this repulsion that drives the formation of a third, very weakly charged, bilayer phase.

Hexagonal lipid–DNA complexes appear in certain regions of the ρ, m plane as soon as k or f_v become sufficiently small, or when the mean spontaneous curvature becomes strongly negative. These two cases are discussed in the following sections.

Soft planar membranes

Although not very abundant, some lipid membranes are characterized by small bending rigidities of only a few k_BT (Lipowsky and Sackmann, 1995). Moreover, the bending rigidity can be substantially reduced by adding short-chain amphiphiles to the lipid mixture (Safinya et al., 1989). Upon lowering k, one expects the appearance of hexagonal lipoplex phases, as indeed observed experimentally (Koltover et al., 1998). Thus, our second-phase diagram was calculated for the limiting case $k = 0$ (in which limit the value of c_0 is irrelevant). We have also set $f_v \equiv 0$. Qualitatively similar results were obtained with $k \approx 1k_BT$ and $c_0^c = c_0^h = 0$.

For infinitely flexible membranes, the relative stability of the various possible phases is fully governed by electrostatics. Thus, for instance, owing to its higher charging energy, the H_{II} phase is always less stable than the L_α phase. In contrast, as shown in previous sections, the H_{II}^C phase is more stable than the L_α^C, but only for a certain range of lipid compositions. Thus, because the electrostatic free energies of the different structures show different dependencies on lipid (CL/HL) and lipid/DNA ratios, the phase diagram is determined by a rather complex interplay between electrostatic energies and chemical composition constraints.

The phase diagram for the system of interest here is shown in Fig. 6, revealing a plethora of phase boundaries and coexistence regimes. Despite its apparent complexity, this phase diagram is not too difficult to explain.

Let us first point out some gross features of the phase diagram. When ρ is small, there are not enough lipid molecules to complex all the DNA strands. Thus, on this side of the diagram, we always find naked DNA (D) coexisting with either S-type (L_α^C) or H-type (H_{II}^C) complexes, or both. Similarly, at high values of ρ, all DNA is already complexed, and the appearance of an excess lipid (here bilayer) phase is unavoidable. Also expected is the complete absence of an H_{II} phase. Whenever lipids are expelled from complexes, they prefer the electrostatically more favorable bilayer (B) phase. We also note the existence of monophasic regions. The sandwich complex (S in the figure) persists over a range of ρ (at high m), reflecting the ability of this structure to tolerate changes in lipid composition by adjusting the DNA–DNA distance, d. Recall that we have not allowed a similar, structural, degree of freedom for the honeycomb structure (H). That is, we have imposed the structural constraint $R_H = R_D + \delta =$ constant. If all lipids and DNA are involved in H-complex formation, this implies the linear relationship $m = [a/2\pi(R_D + \delta + h)b]\rho$. Thus, the monophasic H-phase regime shrinks to a straight line in the phase diagram, as indicated by the dashed curve in Fig. 6. Had we allowed δ to vary, the H-phase line would expand somewhat, yielding a lense-shaped region.

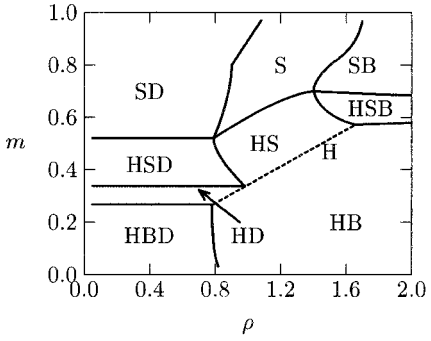

FIGURE 6 The Phase diagram of a lipid–DNA mixture, for lipids that self-assemble into very soft planar membranes. The phase diagram was calculated for membranes characterized by $k = 0$ and $f_v \equiv 0$. The symbols S, B, H, and D, denote, respectively, the L_α^C, L_α, H_{II}^C, and uncomplexed DNA phases. (See Fig. 1.) The straight dashed line marks the single (H_{II}^C) phase region.

In our discussion of the electrostatic properties of the L_α^C and H_{II}^C unit cells, we have concluded that a single H_{II}^C phase becomes unstable with respect to a L_α^C phase for $\phi_H \leq 0.15$. When the possible appearance of other phases is taken into account, the H_{II}^C phase may lose its dominance at even higher values of ϕ_H. Indeed, in Fig. 6, we observe that the H-phase line extends over the range $0.27 \leq m \leq 0.57$, indicating that the H_{II}^C phase is partly dissolved, giving rise to the appearance of two additional phases, (B and D at low m, B and S at high m).

To interpret the more subtle features of the phase diagram, it is important to bear in mind that, whenever two (or three) lipid-containing phases are in equilibrium with each other, their lipid compositions are generally different. The compositional degrees of freedom allow the system to minimize its free energy by optimizing the lipid compositions of the possible phases. To demonstrate these notions, let us follow the phase evolution of the system as we increase ρ, keeping $m =$ constant. Fig. 7 describes the changes in the lipid compositions of the evolving phases along two such lines, $m = 0.31$ and $m = 0.60$.

Along $m = 0.31$ (*solid lines* in Fig. 7), we always find the H_{II}^C phase. From Fig. 3 we know that, for $m = \phi_H = 0.31$, the H_{II}^C complex is more stable than the alternative lipoplex

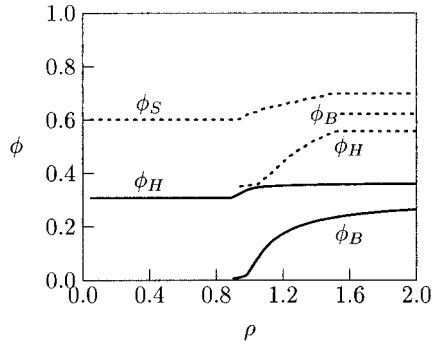

FIGURE 7 The change in the lipid compositions of coexisting phases upon increasing ρ at $m =$ constant in the phase diagram shown in Fig. 6. *Solid curves*, $m = 0.31$; *dashed curves*, $m = 0.6$.

phase, L_α^C. Thus, at low values of ρ, all lipids are accommodated in hexagonal complexes (hence $\phi_H = m$), coexisting with uncomplexed DNA, (region HD in Fig. 6). Upon increasing ρ, a point is reached where all DNA and lipid are complexed. For $m = 0.31$ this happens at $\rho = 2\pi m(R_D + \delta + h)b/a = 0.9$. This point lies on the H phase line in Fig. 6. Immediately beyond this point another, bilayer, phase begins to appear. Because the H_{II}^C complexes are most stable at isoelectricity, $\phi_H = \phi_H^* = 0.345$, they tend to increase their CL content from 0.31 to 0.345. The presence of the extra, bilayer, phase allows them to do so by trading CLs for HLs with the bilayer, as clearly seen in Fig. 7. In fact, for $0.9 < \rho < 1$ nearly all charged lipid are used to increase ϕ_H toward ϕ_H^*, implying a very weakly charged coexisting L_α phase. Once the H_{II}^C phase has reached its optimal composition ϕ_H^* (at about $\rho \approx 1$), it further takes up only a small fraction of cationic lipids to ensure the same chemical potential in both the L_α and H_{II}^C phases. Finally, we note that the phase evolution scenario along $m = 0.31$ is quite similar to the phase progression observed in Fig. 5 (for most values of m). Namely, a two-phase (complex/DNA) region, followed by a one-phase (complex) region and then again a two-phase (complex/bilayer) region. The only difference is that the L_α^C complex is replaced here by the H_{II}^C complex. In Fig. 6, the one-phase region shrinks to a line, because the hexagonal complex does not possess any structural degrees of freedom.

Richer phase evolution is encountered as ρ increases along the $m = 0.6$ line, (*dashed curves* in Fig. 7). In this case, the first complexes to form (i.e., at low values of ρ) are lamellar aggregates. This follows from the fact that, at high CL concentrations, the L_α^C phase is more stable than the H_{II}^C phase. From Fig. 3 we know that, for $m = \phi_S = 0.6$ the DNA–DNA distance in the lamellar complexes must be small, we find $d = 28$ Å. At $\rho \simeq 0.9$, all the DNA is complexed and only L_α^C aggregates are present in solution. For $m = 0.6$, this single phase region (S in Fig. 6) is very narrow, ending at $\rho \simeq 0.95$. Within this region, $d = \rho a/bm$ increases linearly with ρ and $\phi_S = m = 0.6$ is constant. From Fig. 3 we recall that, as d increases (at constant ϕ), there should be a point where the H_{II}^C complex becomes more stable than the L_α^C complex. Thus, an $L_\alpha^C \rightarrow H_{II}^C$ transition should take place at a certain ρ, even if $\phi_S = \phi_H = m =$ constant. Because ϕ_S and ϕ_H need not be the same, the H_{II}^C phase appears already at a smaller value of ρ. The initial composition of the H_{II}^C phase is $\phi_H \simeq 0.35$. As ρ increases further within the HS coexistence region ($0.95 \leq \rho \leq 1.5$) both ϕ_H and ϕ_S increase, implying "overcharging" of the complexes by cationic lipids. Eventually, at $\rho \simeq 1.5$, the lipids prefer the formation of a separate bilayer phase (of composition $m = 0.6$) rather than joining and continuing to overcharge the DNA–lipid complexes.

Koltover et al. (1998) have experimentally studied the phase progression along the isoelectric "dilution line" (lowering m at $\rho = 1$) in a system of soft lipids. Our calculations agree with their results.

Curvature-loving membranes

The last lipid mixture considered here is characterized by the elastic constants: $k = 10k_BT$, $c_0^c = 0$, $c_0^h = -1/25$ Å, and an intersticial energy of $f_v = 0.35k_BT$. In this system, the helper lipid (such as DOPE) prefers the curvature of the H_{II} phase. Yet, because the cationic lipid prefers the planar geometry and because, in the hexagonal geometry, both lipids must pay the chain-stretching penalty, f_v, the elastic energy difference $\Delta f^{el}(\phi) = f_I^{el}(\phi) - f_B^{el}(\phi) = f_H^{el}(\phi) - f_S^{el}(\phi)$ may be either positive or negative, depending on the lipid composition ϕ. (Recall that the elastic energy of the lamellar complex is equal to that of the planar bilayer. Similarly, the elastic energy is the same for both hexagonal phases.) More explicitly, using Eqs. 11 and 12,

$$\Delta f^{el}(\phi) = (ak/2)c_H[c_H - 2c_0(\phi)] + f_v \simeq 1.47\phi - 0.154. \quad (19)$$

The second equality is obtained by substituting the values of the elastic constants mentioned above as well as $a = 70$ Å^2 and $c_H = -1/(R_D + \delta + h) = -1/19$ Å. From Eq. 19, it follows that, elastically, the planar geometry is preferred over the inverse-hexagonal geometry for all compositions exceeding $\phi \approx 0.1$. (The pure helper lipid, $\phi = 0$, indeed prefers the inverse-hexagonal geometry.) Recalling that the electrostatic energy of the H_{II} phase is always larger than that of the L_α phase, a DNA-free inverse-hexagonal phase is only expected to appear at very low values of ϕ.

In contrast, around the isoelectric point of the H_{II}^C phase, its electrostatic energy is lower than that of the L_α^C phase (i.e., $\Delta f^{es}(\phi) = f_H^{es}(\phi) - f_S^{es}(\phi) \leq 0$ around $\phi = \phi_H^* \simeq 0.35$). From the results shown in Fig. 3, we find $\Delta f^{es}(\phi_H^*) \simeq -0.5k_BT$, whereas from Eq. 19, $\Delta f^{el}(\phi_H^*) \simeq 0.35$. Thus $\Delta f(\phi_H^*) = \Delta f^{es}(\phi_H^*) + \Delta f^{el}(\phi_H^*) < 0$, indicating that, just around ϕ_H^*, the hexagonal complexes are more stable than the lamellar ones. Yet, this situation quickly reverses as ϕ deviates from ϕ_H^*. Thus, around the isoelectric point, $\rho = 1$, where all DNA and lipid molecules tend to associate into complexes, we should expect the appearance of H_{II}^C complexes when the total lipid composition, m, is close to ϕ_H^* and lamellar complexes at high values of m. The CL–DNA complexes formed in other regions of the ρ, m diagram will be dictated by the optimal partitioning of the lipids between the various possible phases.

These qualitative considerations are corroborated by the phase diagram shown in Fig. 8. For example, in accordance with the above arguments, we note that the region over which all lipids and DNA are involved in the formation of a (single) H_{II}^C phase is extremely narrow, corresponding to the short dashed line (H) passing through $\rho = 1$, $m = \phi_H^* = 0.345$. The phase behavior around this point is also inter-

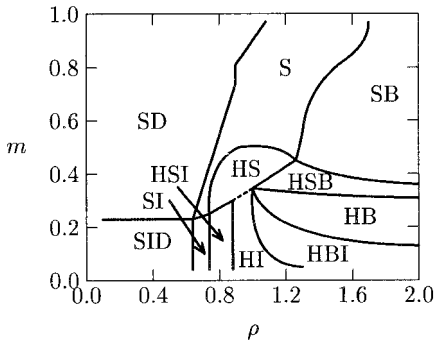

FIGURE 8 The phase diagram of a lipid–DNA mixture involving curvature-loving helper lipid, that is: $c_0^h = -1/25$ Å. The other elastic constants are $k = 10k_BT$, $f_v = 0.35$, $h = 6$ Å, and $c_0^c = 0$. The symbols S, H, B, I, and D denote, respectively, the L_α^C, H_{II}^C, L_α, H_{II}^C, and uncomplexed (naked) DNA phases. The broken line marks the single H_{II}^C phase.

pretable. As m increases (at $\rho \simeq 1$), a small region appears (HS) where lamellar and hexagonal complexes coexist in solution. In this region, the H_{II}^C complexes maintain their optimal composition $\phi_H^* = 0.345$, whereas the L_α^C complexes, whose energy is rather insensitive to lipid composition (Fig. 3), accommodate all other lipids. As we go in the opposite direction, i.e., lowering m (hence enriching the system with HL) at $\rho \simeq 1$ we enter the HI regime where H_{II}^C complexes coexist with an H_{II} lipid phase. Here, again, the H_{II}^C phase maintains its optimal composition whereas the added helper lipids organize in their favorable hexagonal phase H_{II}. The H_{II} phase appears, as expected, in all the low m regions of the phase diagram.

In the high m regime ($m \geq 0.5$), the lipid mixture is rich in CL molecules, implying, by Eq. 19 and Fig. 2, that the L_α^C phase is more favorable than the H_{II}^C phase, both elastically and electrostatically. Similarly, the L_α phase is preferred over the H_{II} phase. Thus, for $m \geq 0.5$, as ρ increases at constant m, we observe the same phase progression, SD $\rightarrow$ S $\rightarrow$ SB, as we found in Fig. 5 (and in Fig. 6 for very large m). Somewhat less obvious, yet not difficult to explain, is the phase behavior on the low ρ side of the phase diagram (say $\rho \leq 0.6$). In this region, there are not enough lipids to complex all the DNA. At high m, the L_α^C phase is more stable than the H_{II}^C phase and, hence, naked DNA (D) coexists with lamellar (S) complexes. For $m \simeq 0.35$, the hexagonal complexes are more stable than the lamellar ones, yet the system prefers the lamellar complexes because, by increasing d, they enable complexation of larger amounts of DNA. Finally, at the bottom-left corner of the phase diagram (low ρ, low m), we observe a three-phase coexistence regime where lamellar complexes (S) coexist not only with an excess DNA phase (D), but also with an hexagonal lipid phase (I). The hexagonal lipid phase consists, essentially exclusively, of neutral helper lipids that not only prefer the hexagonal geometry but also do not contribute to the stability of the lamellar complexes. Thus, the lamellar complex phase is enriched by cationic lipids, as we shall see in Fig. 9 below.

More complex phase behavior is observed in the region $\rho \geq 0.7$, $m \leq 0.5$ of the phase diagram, exhibiting the appearance of H_{II}^C complexes (H), coexisting with various other phases, depending on the exact lipid composition and lipid-to-DNA concentration ratio. The origin of this behavior is the delicate interplay between elastic and electrostatic contributions to the free energies of the L_α^C and H_{II}^C phases, and the ability of the H_{II} and L_α phases to serve as a lipid source (or "dump"). Some of the features characterizing the right-bottom quarter of the phase diagram have already been explained when we discussed the phase behavior around $\rho = 1$ and $m = \phi_H^*$. Additional aspects of this behavior become clearer when we follow the changes in lipid compositions of the various phases along $m =$ constant lines.

In Fig. 9, we follow the phase progression along two, relatively low, $m =$ constant lines; $m = 0.16$ and 0.47. The $m = 0.16$ line starts at the three-phase, SID, region, where lamellar complexes of composition $\phi \simeq 0.23$, (i.e., their CL content is larger than the total CL percentage in the system), coexist with an hexagonal lipid phase composed of HL only ($\phi_I \approx 0$) and an excess DNA phase. At $\rho \simeq 0.6$, all the DNA is complexed. Then, over a narrow range of ρ, the added lipids continue to redistribute between the pure-HL hexagonal phase and the lamellar complexes whose CL content increases slightly to $\phi_S \simeq 0.25$. At $\rho \simeq 0.7$, hexagonal complexes coexist with the lamellar ones, the latter disappearing at $\rho \simeq 0.9$, where $\phi_H \simeq 0.3$. From $\rho \simeq 0.9$, ϕ_H increases linearly, reaching its isoelectric value $\phi_H^* = 0.345$ at $\rho = 1$. Beyond this point, $\phi_H = \phi_H^*$ stays essentially constant as ρ increases, i.e., all the DNA is packed in isoelectric H_{II}^C complexes. The excess lipids are arranged in one or two lipid phases. Just above $\rho = 1$, and as long as $\phi_I \leq 0.02$, the lipids organize in the H_{II} phase; $\phi_I = 0.02$ marks the onset of the $H_{II} \rightarrow L_\alpha$ transition, as shown in Fig. 4. At coexistence, the composition of the L_α phase is $\phi_B \simeq 0.07$, as dictated by the common tangent construction. The $H_{II} \rightarrow L_\alpha$ transition is completed when $\rho \simeq 1.5$, from which

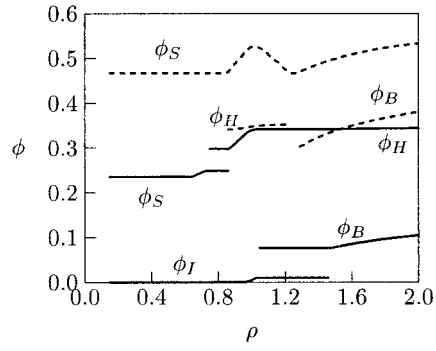

FIGURE 9 The change in the lipid compositions of coexisting phases upon increasing ρ at $m =$ constant in the phase diagram shown in Fig. 8. *Solid curves*, $m = 0.16$; *dashed curves*, $m = 0.47$.

point all the excess lipids go into bilayers. As $\rho \to \infty$, $\phi_B \to m = 0.16$.

The phase progression along the $m = 0.47$ line can be analyzed similarly. One point of special interest here is the reentrant transition S $\to$ HS $\to$ S which, for $m = 0.47$, begins at $\rho \simeq 0.9$ (where the H = H_{II}^{C} phase appears) and ends at $\rho \simeq 1.2$ (where the H phase disappears).

To conclude, in a lipid DNA mixture containing curvature-loving helper lipids, hexagonal complexes are expected to be formed when the cationic lipid content is relatively low and the lipid-to-DNA ratio is high. In this region, the system can optimally adjust the lipid composition of the complexes, expelling the rest of the lipids into excess lipid phases.

CONCLUDING REMARKS

Following recent experiments (Koltover et al., 1998) and qualitative theoretical predictions (May and Ben-Shaul, 1997; Harries et al., 1998), we have presented here a rather detailed analysis of the structural and thermodynamic characteristics of DNA/CL/HL mixtures. This analysis should be useful for the interpretation of future experimental studies and may be relevant for the design of a particular lipoplex geometry.

We have shown that the elastic properties of the lipid membranes used as the lipid source for DNA condensation play an important, albeit not exclusive, role in determining the preferred aggregation geometry of the lipoplex. Qualitatively, using mixed planar membranes (i.e., large vesicles) as the lipid source, the lamellar complex is the optimal structure, provided the membranes are rigid. In contrast, with soft or curvature-frustrated membranes as the lipid source, the preferred aggregation geometry is generally provided by the inverse-hexagonal complex. By frustrated membranes we refer here to bilayers composed of monolayers characterized by negative spontaneous curvature, as is the case, for instance, with DOPE as the helper lipid.

One must remember, however, that more important even than the elastic properties of the lipid membranes are the electrostatic interactions between the lipids and the DNA. Consequently, the preferred complexation geometry is generally dictated by a nontrivial interplay between the electrostatic and elastic contributions to the complex formation free energy. Because both contributions depend on the CL/HL composition, different phases may be favored at different lipid compositions. Still, knowing the lipid composition and the way it affects the relative stability of the lipid–DNA complex does not suffice to determine the nature, number, and proportions of the different phases that appear in solution. This requires an additional, thermodynamic phase, calculation that takes into account all the relevant compositional and structural degrees of freedom of the various possible phases. Of particular importance in this context is the possibility of lipid exchange between different phases. As we have seen, under most conditions, the CL/HL/DNA mixture splits into two or even three phases, involving different proportions of the three chemical species. When more than three components are present in solution, the phase diagram will be even more complex.

Notwithstanding all these complexities, our model calculations suggest that anticipating some gross features of the phase diagram corresponding to a given CL/HL/DNA mixture is not impossible. Namely, certain regions of the phase diagrams can always be predicted with considerable confidence (e.g., the corners of the ρ, m plane and the single-phase regions). Intermediate regions can often be inferred by their bordering regions. Additional insights can be gained from our three generic phase diagrams. We believe that these qualitative conclusions are robust in the sense that they are valid despite the various approximations involved in our theoretical model.

Finally, it must be emphasized that our calculations are only valid for systems in true thermodynamic equilibrium. That is, we have assumed that the systems considered had enough time to exchange lipid molecules between the various possible phases, enabling the total free energy to reach its global minimum. Experimentally, this may not always be the case. Indeed, some experiments indicate the formation of complexes whose symmetries differ from the two basic structures considered here. At the same time, it is important to note that the observation of two or three coexisting structures is by no means an indication that the system is not already equilibrated.

We thank Cyrus Safinya, Joachim Rädler, and Bill Gelbart for helpful discussions. We also thank the Israel Science Foundation (grant 8003/97) and the US–Israel Binational Science Foundation (grant 97-205) for financial support.

S.M. thanks the Minerva foundation for a post-doctoral Fellowship and D.H. the Clore Foundation for a doctoral Fellowship. The Fritz Haber Center is supported by the Minerva Foundation, Munich, Germany.

REFERENCES

Andelman, D., M. M. Kozlov, and W. Helfrich. 1994. Phase transitions between vesicles and micelles driven by competing curvature. *Europhys. Lett.* 25:231–236.

Battersby, B. J., R. Grimm, S. Hübner, and G. Cevc. 1998. Evidence for three-dimensional interlayer correlations in cationic lipid–DNA complexes as observed by cryo-electron microscopy. *Biophys. Biochim. Acta.* 1372:379–383.

Boukhnikachvili, T., O. AguerreChariol, M. Airiau, S. Lesieur, M. Ollivon, and J. Vacus. 1997. Structure of in-serum transfecting DNA-cationic lipid complexes. *FEBS Lett.* 409:188–194.

Bruinsma, R. 1998. Electrostatics of DNA-cationic lipid complexes: isoelectric instability. *Eur. Phys. J. B.* 4:75–88.

Chen, Z., and R. P. Rand. 1998. Comparative study of effects of several *n*-alkanes on phospholipid hexagonal phases. *Biophys. J.* 74:944–952.

Felgner, P. L. 1997. Nonviral strategies for gene therapy. *Sci. Am.* 276: 102–106.

Felgner, P. L., T. R. Gadek, M. Holm, R. Roman, H. W. Chan, M. Wenz, J. P. Northrop, G. M. Ringold, and M. Danielsen. 1987. Lipofectin: a

highly efficient, lipid-mediated DNA transfection procedure. *Proc. Natl. Acad. Sci. USA.* 84:7413–7417.

Gawrisch, K., V. A. Parsegian, D. A. Tate, M. W. Hajduk, S. M. Gruner, N. L. Fuller, and R. P. Rand. 1992. Energetics of a hexagonal–lamellar–hexagonal phase transition sequence in dioleoylphosphatidylethanolamine membranes. *Biochemistry*. 31: 2856–2864.

Harries, D., S. May, W. M. Gelbart, and A. Ben-Shaul. 1998. Structure, stability and thermodynamics of lamellar DNA-lipid complexes. *Biophys. J.* 75:159–173.

Helfrich, W. 1973. Elastic properties of lipid bilayers: theory and possible experiments. *Z. Naturforsch.* 28:693–703.

Hope, M. J., B. Mui, S. Ansell, and Q. F. Ahkong. 1998. Cationic lipids, phosphatidylethanolamine and the intracellular delivery of polymeric, nucleic acid-based drugs (review). *Mol. Memb. Biol.* 15:1–14.

Hübner, S., B. J. Battersby, R. Grimm, and G. Cevc. 1999. Lipid–DNA complex formation: reorganization and rupture of lipid vesicles in the presence of DNA as observed by cryoelectron microscopy. *Biophys. J.* 76:3158–3166.

Hui, S. W., M. Langner, Y-L. Zhao, R. Patrick, E. Hurley, and K. Chan. 1996. The role of helper lipids in cationic liposome-mediated gene transfer. *Biophys. J.* 71:590–599.

Kirk, G. L., S. M. Gruner, and D. L. Stein. 1984. A thermodynamic model of the lamellar to inverted hexagonal phase transition of lipid membrane–water systems. *Biochemistry.* 23:1093–1102.

Koltover, I., T. Salditt, J. O. Rädler, and C. R. Safinya. 1998. An inverted hexagonal phase of cationic liposome-DNA complexes related to DNA release and delivery. *Science.* 281:78–81.

Kozlov, M. M., S. Leikin, and R. P. Rand. 1994. Bending, hydration and interstitial energies quantitatively account for the hexagonal–lamellar–hexagonal reentrant phase transition in dioleoylphosphatidylethanolamine. *Biophys. J.* 67:1603–1611.

Lasic, D. D. 1997. Liposomes in Gene Delivery. CRC Press, Boka Raton, FL.

Lasic, D. D., H. Strey, M. C. A. Stuart, R. Podgornik, and P. M. Frederik. 1997. The structure of DNA–liposome complexes. *J. Am. Chem. Soc.* 119:832–833.

Leikin, S., M. M. Kozlov, M. M. Fuller, and R. P. Rand. 1996. Measured effects of diacylglycerol on structural and elastic properties of phospholipid membranes. *Biophys. J.* 71:2623–2632.

Lekkerkerker, H. N. W. 1989. Contribution of the electric double layer to the curvature elasticity of charged amphiphilic monolayers. *Physica A.* 159:319–328.

Lipowsky, R., and E. Sackmann, (eds). 1995. Structure and Dynamics of Membranes. Elsevier, Amsterdam.

May, S. 1996. Curvature elasticity and thermodynamic stability of electrically charged membranes. *J. Chem. Phys.* 105:8314–8322.

May, S., and A. Ben-Shaul. 1995. Spontaneous curvature and thermodynamic stability of mixed amphiphilic layers. *J. Chem. Phys.* 103: 3839–3848.

May, S., and A. Ben-Shaul. 1997. DNA-lipid complexes: stability of honeycomb-like and spaghetti-like structures. *Biophys. J.* 73: 2427–2440.

Parsegian, V. A., and D. Gingell. 1972. On the electrostatic interaction across a salt solution between two bodies bearing unequal charges. *Biophys. J.* 12:1192–1204.

Pitard, B., N. Oudrhiri, J. P. Vigneron, M. Hauchecorne, O. Aguerre, R. Toury, M. Airiau, R. Ramasawmy, D. Scherman, J. Crouzet, J. M. Lehn, and P. Lehn. 1999. Structural characteristics of supramolecular assemblies formed by guanidinium-cholesterol reagents for gene transfection. *Proc. Natl. Acad. Sci. USA.* 96:2621–2626.

Rädler, J. O., I. Koltover, T. Salditt, and C. R. Safinya. 1997. Structure of DNA–cationic liposome complexes: DNA intercalation in multilamellar membranes in distinct interhelical packing regimes. *Science.* 275: 810–814.

Rädler, J. O., I. Koltover, A. Jamieson, T. Salditt, and C. R. Safinya. 1998. Structure and interfacial aspects of self-assembled cationic lipid-DNA gene carrier complexes. *Langmuir.* 14:4272–4283.

Safinya, C. R., E. B. Sirota, D. Roux, and G. S. Smith. 1989. Universality in interacting membranes: the effect of cosurfactants on the interfacial rigidity. *Phys. Rev. Lett.* 62:1134–1137.

Salditt, T., I. Koltover, J. O. Rädler, and C. R. Safinya. 1997. Two dimensional smectic ordering of linear DNA chains in self-assembled DNA–cationic liposome mixtures. *Phys. Rev. Lett.* 79:2582–2585.

Seddon, J. M., and R. H. Templer. 1995. Polymorphism of lipid–water systems. *In* Structure and Dynamics of Membranes, 2d ed, Vol. 1. R. Lipowsky and E. Sackmann, editors. Elsevier, Amsterdam. 98–160.

Sternberg, B. 1996. Morphology of cationic liposome/DNA complexes in relation to their chemical composition. *J. Liposome Res.* 6:515–533.

Sternberg, B., F. L. Sorgi, and L. Huang. 1994. New structures in complex formation between DNA and cationic liposomes visualized by freeze-fracture electron microscopy. *FEBS Lett.* 356:361–366.

Szleifer, I., D. Kramer, A. Ben-Shaul, D. Roux, and W. M. Gelbart. 1988. Curvature elasticity of pure and mixed surfactant films. *Phys. Rev. Lett.* 60:1966–1969.

Tarahovsky, Y. S., R. S. Khusainova, A. V. Gorelov, T. I. Nicolaeva, A. A. Deev, A. K. Dawson, and G. R. Ivanitsky. 1996. DNA initiates polymorphic structural transitions in lecithin. *FEBS Lett.* 390:133–136.

Templeton, N. S., D. D. Lasic, P. M. Frederik, H. H. Strey, D. D. Roberts, and G. N. Pavlakis. 1997. Improved DNA: liposome complexes for increased systemic delivery and gene expression. *Nature Biotech.* 15: 647–652.

Verwey, E. J. W., and J. T. G. Overbeek. 1948. Theory of the Stability of Lyophobic Colloids. Elsevier, New York.

Wagner, K., E. Keyes, T. W. Kephart, and G. Edwards. 1997. Analytical Debye–Hückel model for electrostatic potentials around dissolved DNA. *Biophys. J.* 73:21–30.

Wagner, K., D. Harries, S. May, V. Kahl, J. O. Rädler, and A. Ben-Shaul. 2000. Direct evidence for counterion release upon cationic lipid-DNA condensation. *Langmuir.* 16:303–306.

Zuidam, N. J., D. H. Lerner, S. Margulies, and Y. Barenholz. 1999. Lamellarity of cationic liposomes and mode of preparation of lipoplexes affect transfection efficiency. *Biophys. Biochim. Acta.* 1419:207–220.